INTERNATIONAL ATOMIC ENERGY AGENCY
UNITED NATIONS EDUCATIONAL, SCIENTIFIC AND CULTURAL ORGANIZATION
INTERNATIONAL CENTRE FOR THEORETICAL PHYSICS
I.C.T.P., P.O. BOX 586, 34100 TRIESTE, ITALY, CABLE: CENTRATOM TRIESTE

H4.SMR/452-51

ADRIATICO CONFERENCE ON FOURIER OPTICS AND HOLOGRAPHY

INTERFEROMETRY

Prof. H. J. Tiziani

University Stuttgart

INTERFEROMETRY

H.J.Tiziani
University Stuttgart

Introduction to two–beam interferometry

Fringe analysis

Heterodyne interferometry

Phase locked technique

Applications

INTERFEROMETRY

by H.J. Tiziani

1. Introduction

Basic interferometry and holographic interferometry are becoming useful tools for precision measurements. The use of electronic solid state detector arrays, microprocessors, and computers for extracting information from the interferograms improves its applications. Computer analysis is becoming increasingly important. Much more information can be extracted from the interferograms leading to higher sensitivities and accuracies.

The techniques become very useful for industrial applications, for contactless surface and deformation measurements as well as for strain, displacement, and vibration analysis and flow measurements. Heterodyne interferometry is one of the interferometric measuring techniques which make use of a reference beam shift or modulation to get high precision.

The fringe analyzing procedures including fringe peak detection and fringe order determination are tedious and time consuming. Automatic fringe analysis and precision phase measuring techniques are very important in applying interferometric techniques. Automatic quantitative evaluation of interferograms require accurate interference phase measurements, independent of fringe position and intensity variations superposed onto the interferograms. In many interferometric arrangements, phase shifting or heterodyne techniques have been introduced for automatic fringe analysis.

In the phase shifting technique or quasi-heterodyne technique the relative phase is changed continuously or stepwise, using at least three phase shifts of 90 or 120 degrees for instance. The phase of the interference patterns can then be computed from the different measured intensity values. The phase shifting technique is very appropriate for digital processing and TV techniques. Interferometry and two reference beam holography together with video electronic processing lead to a sensitivity of 1/100 of a fringe at any point of the fringe pattern in the TV image. In heterodyne methods the relative phase increases linearly in time and the reference phase is measured electronically at the beat frequency of the reconstructed wavefields. Heterodyne interferometry and holographic interferometry offer high spatial resolution and interpolation up to 1/1000 of a fringe. It requires, however, sophisticated electronic equipment and mechanical scanning of the fringe pattern /10/.

An automatic fringe analysis leads to the wavefront. Polynomials are very useful for error as well as for system analysis.

With the overheads F_1 - F_6 the principle of Interferometry will be discussed. The Fizeau and Twyman Green arrangements are the set ups mainly used. There are of course many other configurations to be applied.

2. Automatic fringe analysis and phase measuring interferometry

The introduction of the laser in 1960 and the progress made the last years in automatic fringe analysis are mostly responsible for the wide-spread application of interferometry in industry today. Some methods and applications will be discussed briefly for two beam interferometry. Fringe analysis will be similar in holography, speckle application and moiré techniques. The superposition of the two wavefields $a_1 \cos[\omega t - \phi_1(\vec{x})]$ and $a_2 \cos[\omega t - \phi_2(\vec{x})]$ lead to the intensity

$$I(x) = I_o \left[1 + m\cos\phi(\vec{x})\right] \qquad 1)$$

where $\phi(\vec{x}) = \phi_1(\vec{x}) - \phi_2(\vec{x})$ $\qquad I_o = |a_1|^2 + |a_2|^2$ and
m = modulation of interference fringes, $\phi(\vec{x}) = n(\vec{x})\,\vec{k}\cdot\vec{x}$
with $\vec{k}$ as the wavevector of the light,
$|k| = \frac{2\pi}{\lambda}$ and n as refractive index and x the space coordinate.

Position, displacement, vibration amplitudes and refractive index variations can be found. From the detector signal of an interference arrangement the phase ϕ can be determined. There are in different ways the following problems to be investigated

- three unknown: I_o, m, ϕ
- ϕ is determined to a factor of 2π only
- sign ϕ.

In addition, the accuracy can be drastically increased by an appropriate interpolation technique. Digital interferometry provides means for obtaining very precise measurements at rapid rates. For the fringe analysis many different methods are applied. They can be classified into static and dynamic methods[1-8].

3. Fringe analysis with static techniques

For the fringe analysis with static methods a tilt is often introduced to avoid closed fringes. The fringe centers can be found manually and by using a digitizing tablet as well as by using video- and image processing techniques.

To estimate fringe peaks, the fringe density binarization technique is commonly used in many fringe analysis systems because of simple algorithms. The grey level method where local variation of fringe density is considered, is sensitive to noise, but can detect peaks by processing only local areas smaller than those in the binary case. In order to extract fringe peaks in the grey level method, it is very important to diminish the influence of noise, including speckle noise. A simple and effective way is unweighted averaging.

The carrier fringe analysis in the spatial domain using Fourier techniques can be very useful. The Fourier-transformation technique was first proposed by Takeda[1] and extended by Kreis[2]. Equation 1 can be rewritten as

$$I(x,y) = A(x,y) + B(x,y)\cos\left[\phi(x,y) + \frac{2\pi}{\lambda}\sin\vartheta\right] \qquad 2)$$

where the bias phase is introduced by a tilt ϑ into an interferometric fringe pattern. Equation 2 can be written as

$$I(x,y) = A(x,y) + C(x,y)\exp\left[i\frac{2\pi}{\lambda}x\sin\vartheta\right] + C^*(c,y)\exp\left[-i\frac{2\pi}{\lambda}x\sin\vartheta\right]$$

where $C(x,y) = \frac{1}{2}B(x,y)\exp\left[i\phi(x,y)\right]$, $C^*(x,y)$ is complex conjugate.

In the Fourier domain analysis, the conjugate carrier fringe pattern is Fourier transformed to obtain

$$\tilde{I}(f_x,f_y) = \tilde{A}(f_x,f_y) + \tilde{C}(f_x-f_o,f_y) + \tilde{C}^*(f_x+f_o,f_y)$$

where $\tilde{I}$, $\tilde{A}$, $\tilde{C}$, $\tilde{C}^*$ are the Fourier tranaforms of I, A, C, C^*. If the tilt introduced is appropriate, the terms $\tilde{A}$, $\tilde{C}$, $\tilde{C}^*$ are separated in the Fourier domain. The term $\tilde{C}(f_x-f_o,f_y)$ has the information of the phase $\phi(x,y)$, shifting it mathematically to the origin of the Fourier domain we obtain the term $\tilde{C}(f_x,f_y)$ which in turn Fourier transformed back leads to C(x,y). It can easily be seen that the imaginary part of its logarithm leads to the phase $\phi(x,y)$ as follows

$$\ln C(x,y) = \ln\frac{B(x,y)}{2} + i\phi(x,y) \qquad 3)$$

Fig. 1 shows the procedure of the phase detection in the spatial domain using Fourier transformation. Care needs to be taken when filtering $\tilde{C}(f_x,f_y)$ for cleaning up the fringe pattern for not taking away useful information.

In fig. 2 a typical fringe analysis with the Fourier Transformation method is demonstrated to compare the surface topography.

Fig. 1a shows the fringe pattern of a two beam interference arrangement (Fizeau) and fig. 2b and fig. 2c the representation of wavefront (surface topography compared with a spherical surface in pseudo 3-D representation and contour lines respectively. The contour lines correspond to height variation of 0,544 µm. Furthermore from equation 4, $\phi(x,y)$ can be calculated at each point

$$\phi(x,y) = \arctan\frac{I_m[C(x,y)]}{R_e[C(x,y)]} \qquad 4)$$

The signs of the numerat or and the denominator have to be taken into account separately to obtain values ranging from $-\pi$ to π.

The ambiguities of 2 π can be overcome by complementary informations. The sign ambiguity may be overcome by the detection of slope changes, the sign reversal points can be detected by using two reconstructions with an arbitrary phase shift between.

The Fourier-transform method usually does not require phase shifts. By a pointwise analysis the determination of phase variations even in sub-wavelength range is obtained from one interferogram. The method can be very valuable in holographic interferometry.

Fig. 2 shows a typical example of a fringe analysis with the described Fourier-transform technique. The same surface again investigated interferometrically with a Fizeau-arrangement was analysed with the phase shift technique (Fig. 5).

4. Fringe analysis with dynamic techniques

For dynamic algorithms the relative phase between the reference beam and the test beam in an interferometer is varied at constant, controlled rate or in steps of 90 or 120 degrees for instance.[3-9]

Dynamic techniques are:

- phase shifting in three or four or more steps or continuously
- heterodyne technique
- phase-locked technique

4.1 Phase shifting techniques

The intensity of the interference pattern can be written as

$$I_{m(x,y)} = I_o(x,y) \left\{ 1 + m(x,y)\cos \left[\phi(x,y) + \Delta k \right] \right\} \qquad 5)$$

$\phi x,y) = \frac{2\pi}{\lambda} \cdot W(x,y)$ is the phase distribution of the wavefront W(x,y) across the interference pattern to be measured and Δ is the deliberately introduced phase shift. k = 1,2,3 .... N depending on the number of phase shifts introduced.
The interference pattern can be recorded by a solid state detector array. For the shifting technique at least three patterns with the appropriate phase shifts need to be recorded. Applying for the phase shifts $(-\frac{3\pi}{4}, -\frac{\pi}{4}, \frac{\pi}{4}, \frac{3\pi}{4})$, the phase of the wavefront computed from the four interferograms is:

$$\phi(x,y) = \tan^{-1} \frac{I_4(x,y) - I_2(x,y)}{I_1(x,y) - I_3(x,y)} \qquad 6)$$

For accurate phase analysis, the phase shifts introduced by a piezo element for instance need to be measured or the piezo be calibrated. An error of λ/10 in the wavefront occurs by an error in the phase shift of 20 per cent. Care needs to be taken when phase shifts in strongly diverging or converging beams are necessary. Schwider proposed a 4 step phase shift procedure with an averaging algorithm, namely

$$\phi(x,y) = \frac{1}{2}\left\{\tan^{-1} \frac{I_3(x,y)-I_2(x,y)}{I_1(x,y)-I_2(x,y)} + \tan^{-1} \frac{I_4(x,y)-I_3(x,y)}{I_2(x,y)-I_3(x,y)}\right\} \qquad 7)$$

It leads to a reduction of errors introduced by an inaccurate phase shifting.

Furthermore the phase stepping could be anything between 0 and π degrees. By the integrating bucket-technique[6,7] the intensity of the fringe pattern is integrated in buckets while the phase is being shifted.

For high accuracy measurements of flat and spherical surfaces, it is useful to work with very few fringes. A phase calculation-algorithm with five measurements of intensity is desirable. The corresponding phase steps are -2Δ, -Δ, 0, 2Δ. For $\Delta = 90^0$ we obtain

$$\tan\phi = \frac{2(I_2-I_4)}{2I_3-I_5-I_1} \qquad 8)$$

The preliminary calibration of the PZT to ensure that the phase step is approximately equal to 90^0 can be carried out with four out of five values of intensity,[5] namely

$$\cos\Delta = \frac{I_5 - I_1}{2(I_4 - I_2)} \qquad 9)$$

Because the five interferogram method is not so much affected by phase stepping errors it is particularly interesting in a Fizeau arrangement where for different aperture heights, different phase shifts occur when shifting the test surface or the reference.

Examples of fringe analysis of a surface in a Fizeau arrangement are shown in fig. 2a and 5. The fringe analysis of the interferogram in fig. 5 obtained with a Fizeau arrangement is based on phase shifting with five phase steps. Fig. 5a shows the fringe pattern and 5b the pseudo 3-D plot and fig. 5c the contour lines respectively. A very good agreement between the static and dynamic technique with fringe shifting was obtained. By the Fourier-method closed fringes should be avoided. Fig. 6 shows schematically a typical hardware we use for our fringe analysis.

Digital interferometry is very useful for getting the interferometric data into a computer for the analysis. An experimental arrangement is shown in fig. 3. For the automatic analysis of closed fringes a phase shift technique is appropriate. Phase shifts can be introduced for instance by tilting a plane-parallel plate, moving a mirror by means of piezo elements or by means of polarization techniques. In fig. 4 a diamond turned Germanium spherical surface is analysed showing shape errors. In fig. 4a fringe patterns with different tilts introduced are shown and in fig. 4b one-dimensional fringe analysis of fig. 4a with tilt compensation. The quasi micro-roughness analysis obtained by the fringe analysis of the same interferogram is shown in fig. 4c. The sensitivity obtained is $\lambda/100$.

For microprofile measurements, stylus instruments are among the most highly developed means of profiling precision surfaces. Interferometry with fringe analysis can be used for micro-structure analysis. An adapted interference arrangement with high numerical aperture NA=0,9 is shown in fig. 7b. A piezo element is used to shift the phase by displacing the beam splitter in steps. A diode array of 500 x 580 elements was used for the study of the CD-disk with a pitch of 0,6 µm shown in fig. 8.

Very often it is useful to describe the wavefront by polynomials. Zernike polynomials are useful because of their orthogonal properties. For special applications Zernike-Tatian-polynomials (for system with central obstruction) or Tschebyscheff polynomials are useful.

4.2 Heterodyne techniques

In interferometry, phase differences of optical fields are transformed into detectable intensity variations. In heterodyne-Interferometry the time dependent phase variation is analysed in the frequency space. The two light fields are assumed to be

$$A_1 = a_1 \cos[\omega t + \phi_1(x,y)]$$

and

$$A_2 = a_2 \cos[\omega t + \Delta\omega t + \phi_2(x,y) + \phi(x,y,t)] \qquad 10)$$

where $\Delta\omega$ is proportional to the frequency shift $f_2 - f_1$ and $\phi(t)$ is the time varying phase shift leading to a frequency shift by interference of the two wave-fields namely

$$I(x,y) = I_o\{1 + m(x,y)\cos[\Delta\omega t + \phi(x,y,t) + \phi_2(x,y) - \phi_1(x,y)]\} \qquad 11)$$

from where the time varying phase variation $\phi(x,y,t)$ can be detected.

The Doppler shift frequency is

$$\delta f = \frac{\phi(x,y,t)}{2\pi t} = \frac{2}{\lambda}\frac{dz}{dt} \qquad 12)$$

where z is the displacement projected parallel to the line of sight, namely

$$z = \frac{\lambda}{2}\int_{t_1}^{t_2} \delta f \, dt$$

It is basically the concept of the well known HP interferometer. For a harmonically oscillating object, $\phi(x,y,t) = \frac{4\pi\cdot\rho}{\lambda}\cos(\Omega t)$ producing a frequency modulated output signal at the detector with carrier frequency of $\frac{\Delta\omega}{2\pi}$ and amplitude and frequency of oscillation of ρ and Ω respectively. The signal can be evaluated by well known frequency analysis techniques.[10]

Fig. 9 shows schematically a two beam heterodyne interferometer arrangement we use for microprofile measurement. The two orthogonal polarized beams of frequency f_1 and f_2 are obtained by the magnetic field in the resonator (Zeemansplitting). The difference frequency of 2 MHz is detected by Det. 1. The height variation Δz

is recorded by detector 2 (Det. 2). A polarizing beam splitter separates the waves with the frequencies f_1 and f_2. The frequency f_2 is modified by the height variation. After passing twice the quarter wave plates R_1, R_2 the beams are recombined and finally compared with the instrumental frequency shift. High numerical aperture lenses are needed for large slopes of the rough surfaces. For slope compensation a double pass arrangement is used as indicated in fig. 9 by DP.

Fig. 10 shows a typical result obtained. Resolutions of 1 µm lateral and 0,5 nm in depth were obtained by scanning a mirror like surface. Depth resolutions of 0,1 nm and better were reported by a reduced lateral resolution.[11] Heterodyne techniques are for time being the most promising methods for contactless high resolution microprofile analysis.[11-13] Other techniques will be developed to be robust for industrial applications with an extended range.

The relation of the measured heights, determined with different techniques, to the commonly used characterization of surfaces in industry needs to be investigated further. The definition used will be given below. New standards may be needed.

A similar arrangement to the one shown schematically in fig. 11 was used for the vibration and noise analysis of rotating car-tyres. The frequency shift of 40 MHz was introduced by the Bragg cell. The frequency analysis perpendicular to the surface at a single point of the side wall is shown in fig. 12. For comparison the result from an independent measurement obtained with a microphone is indicated by the dotted lines in fig. 12. Close agreement was found between the noise detected with a microphone and the analysis of mechanical vibrations when air-pumping was small.[14] By comparison, a result of double pulse holography of the rotating car-tyre is shown in fig. 20.

Heterodyne interferometry will lead to very useful future applications in precision measurements. For the vibration analysis at given points, heterodyne interferometry gives not only the amplitude component of vibration parallel to the line of sight but also the frequency. Furthermore, it can be very useful for the fringe analysis in holographic interferometry. It can be used to relate the holographic interference fringes to a known amplitude of vibration at a selected point obtained by a heterodyne technique. Furthermore, the heterodyne technique can be extended to speckle interferometry for vibration analysis.

By contrast, the laser Doppler velocimeter is used to measure flow of gases and liquids, using the light scattered from small particles suspended in the flowing medium. The speed of optically rough surfaces can be determined by similar methods.

Heterodyne interferometry was extensively treated by Dändliker[1] among others and applied to heterodyne profilometry recently by Huang[11] and others.[12,13]

Heterodyne interferometry is used for distance measurement as well as for microstructure analysis based on scanning the object point by point. The technique can also be applied for fringe analysis in holographic interferometry.

Shearing and two wavelength techniques are very valuable for tesing steep surface such as aspheres. Using two λ-technique a variable measurement sensitivity is attainable, with a resulting wavelength larger than the individual. Two-wavelength interferometry can be used for ranging and contouring at reduced sensitivity. Recently, two wavelength heterodyne interferometry has been reported to be applied for smooth and to some extend for rough surface. By the availability of multiple wavelength laser and of tunable diode-lasers as light sources, multiple wavelength interferometry with small wavelength differences is becoming very interesting for practical applications. Using two wavelength λ_1 and λ_2, the effective difference wavelength is $\Lambda = \lambda_1\lambda_2/(\lambda_1-\lambda_2)$ without being obliged to have interferometric stability at the optical wavelength λ_1 and λ_2 itself and to separate this wavelength optically. This is of great importance for future range finding and industrial distance measuring.

Interferometry for Roughness-Measurements

In the interferometric method described so far applications for surface roughness measurements were indicated. Up today surface roughness is measured by stylus instruments where the displacement of a mechanical control element is measured. The surface contacting element has a radius of a few micrometers and a surface pressure not always negligible. Therefore, contactless measuring techniques are desirable.

For roughness-measurements the height variation can be represented by mean roughness R_a or by the rout-mean-square roughness R_q or the variance

$$R_a = \frac{1}{N}\sum_{i=1}^{N}|z_i| \qquad R_a = \frac{1}{L}\int_0^L z(x)dx$$

$$R_q = \left\{\frac{1}{N}\sum_{i=1}^{N} z_i^2\right\}^{\frac{1}{2}} \qquad R_q = \sqrt{\frac{1}{L}\int_0^L z^2(x)dx} \qquad 13)$$

$$\sigma_z = \left\{E\langle z_i^2\rangle\right\}^{\frac{1}{2}}$$

For the characterization of extremely smooth surface total integrated and angle-resolved scattering, styles profilometry and heterodyne profilometry have been used. Scattering methods lead to statistical information about the surface and are none-contact. By contrast surface damage is risked with contacting stylus profilometers. Heterodyne profilometers can give height resolution in the order of 0,1 nm with a lateral resolution limited by diffraction to 1 µm. Care needs to be taken when the results obtained with different techniques need to be compared. Further investigations are needed because the results do not yet agree.

4.3 Phase locked technique

A phase locked technique will be discussed in connection with one of our applications for subsurface material analysis. For nondestructive material analyses, photoacoustic and photothermal methods can be applied.[15] In photothermal interferometry the thermal expansion of the specimen is measured rather than the thermal wave itself.[16] Fig.13 shows an experimental arrangement where a modulated Ar^+ laser heats the object under test leading to a heat wave that propagates through the material and deforms the surface a few nanometers. An interference arrangement detects the deformation using a phase locked technique, where the piezo shifts the phase appropriately. The intensity at the detector of a two beam interference arrangement can be written according to fig. 13

$$I_S = I_O[1+m\cos\phi] \qquad 14)$$

where

$$I_O = \frac{I_{max} + I_{min}}{2}$$

$$m = \frac{I_{max} - I_{min}}{I_{max} + I_{min}}$$

with I_{max} the maximal intensity, I_{min} the minimum intensity and the phase $\phi = \frac{4\pi}{\lambda} W$, where W is the optical path difference. The optical path difference introduced by thermal expansion is a few nanometers only. Care needs to be taken to adjust the interferometer in order to work in the linear region with maximum positive gradient near P in fig. 13. This is important for maximum sensitivity, minimum adjustment time and ambiguity of a lock-in amplifier. Furthermore, the cosine changes into a sine.

Since $W = W_T + W_r + W_p$ with the thermal expansion W_T, the specimen's surface roughness W_r and the piezo crystal displacement W_p.

By a computer control of the piezo crystal, namely

$$W_p = \frac{3}{8}\lambda_s - W_r$$

the surface roughness is compensated and the interferometer works in the linear region.

For a small thermal expansion

$$I_s = I_o\left[1 + m\frac{2\pi}{\lambda_s} W_T\right]$$

Phase locked techniques are capable of detecting phase differences in two beam arrangements of $\lambda/100$ and may be used for measuring surface topography and subsurface defects. The interferometer incorporates, as part of a servo system, a piezoelectrically driven mirror that is capable of applying a known optical phase offset and a periodic optical modulation. The ac signal is processed to generate an error signal for the servo system. A signal proportional to the phase difference between two beams occurs.

A two beam interferometer using a HeNe Laser is shown in fig. 14 for the analysis of subsurface defects by measuring the small surface deformation caused by a chopped, focused laser beam with the wavelength λ (argon laser λ_2 = 488 nm). The interferometer arrangement is not very sensitive to vibration occuring by scanning the object. The computer controlled piezo-element compensates the surface roughness and adjusts the interferometer to work in

the linear region with maximum positive gradient. It leads to the maximum sensitivity and minimum adjustment time of the lock-in amplifier. A result is shown in fig. 15 where a 3 mm thick Al-plate with holes of 0,8 mm diameter was analysed. The phase measuring indicates clearly the disturbance in the material. The chopper-frequency varied from 20 to 140 Hz. A modified configuration was used to study opaque materials in reflection.

Increasing the chopping frequency from a few hundert Hz to a few MHz leads to a very sensitive subsurface defect analysis by a reduced depth range of course.

5. Application of computer generated holograms

Computer generated holograms are applicable for generating threedimensional images from calculated holograms. They can be useful for optical filtering as well as for testing aspheric surfaces. Holographic optical elements (HOE) are already used as beam splitters and diffraction elements as well as deflection and focussing elements in laser scanners. HOE are recorded by using plane and spherical waves as well as by means of computer generated holograms.

The HOE recorded by superposition of an object- and a reference wave. The object wave can be reconstructed by illumination the hologram after processing with a reconstruction wave similar to the reference.

In generating the computer generated hologram (CGH) an exact analogy to the optically recorded hologram can be made. The distribution in the hologram plane is calculated, the reference wave added, the sum squared, and the result plotted. Sometimes this output needs to be photoreduced to provide a transparency for wave reconstruction. CGH's can be applied for testing aspheric surfaces with high precision.

Aspherical optical surfaces are today and will be even the next years more frequently introduced into optical systems to improve the performance and to reduce the number of optical elements especially in image formation in the infrared. Recently aspheric single lenses were introduced to replace optical systems consisting of 3 to 4 elements in CD players.

Aspheric surfaces can be tested by a point analysis together with 3-dimensional measuring device to generate the surface profile. Interferometric methods such as null test methods or shearing techniques as well as the application of holographic techniques and computer generated holograms are very useful for high precision measurements.

CGH's can be used to compensate or compare complicated wavefronts for different applications. The CGH in a Twyman-Green experimental arrangement as shown in fig. 16 can be used to compensate the aspheric wavefront reflected by the lens under test, for instance. Illuminating the CGH with the perfect aspheric wafefront computed from the optical data leads, after diffraction, to a perfect plane wave to be compared with the perfect reference plane wave from the reference beam reflected from mirror MS. The interference fringes to be analysed are a measure of the discrepancy of the test lens from the data of the aspheric component or surface. Alternatively, an aspheric wave front can be reconstructed from the CGH to be compared with the actual wavefront.

The principle of CGH is not new. Wyant among other described the technique in chapter 13 in optical shop testing (Reference 3). It's application for the accurate, absolute test of steep aspheric surfaces as well as the generating of CGH needed to be improved.

For plotting CGH's a calcomp plotter can be used, in addition different techniques have been deviced or are in the process of being developed such as the use of electron beam scanners. We apply a computer driven Optronics drum scanner. A two beam interference arrangement for an off-axis hologram for testing aspheric surfaces is shown in fig. 16. The incidient wave is separated by the beam splitter into the reference beam reflected back from the mirror MS slightly obliquely and passing through the hologram undisturbed and the test beam. For the fringe analysis one of the previously described techniques can be used. Because closed fringes need to be analysed we prefer the phase shifting technique with phase steps of $\pi/2$. The simple lenses L_1, L_2, L_3 in fig. 16 are auxiliary lenses to adapt the aperture of the lens under test TS. They should also image the test surface onto the CGH, a necessary condition for strong

aspheric wavefronts. Furthermore they can also be used to compensate partly the aspheric wavefront. L_4 is a high quality lens to be used for testing aspherical as well as spherical lense. In addition L_4 and L_1' are used for focussing on the surface unter test as well as for testing spherical surfaces with the same instrument. Furthermore, the accurate position of the vertex for spherical and aspherical surfaces is obtained with L_1' in place generating a perfect spherical wave.

Although the auxiliary lenses need not to be perfect a hologram is computed at first for a known spherical or aspherical surface; the fringe analysis leads to an almost compensation of the errors involved which in turn are compensated when computing the CGH for the test surface.

Adjustment in an industrial test procedure can be time consuming and difficult because 7 degrees of freedom need to be balanced such as tilt and decentring in two directions of the test surface as well as decentring and rotation of the hologram; some of the adjustment errors have similar effects on the interference pattern.

Using the previously described automatic fringe analysis it was found appropriate to approximate the measured wavefront $W(r,\theta)$ by a set of polynomials. Zernike polynomials were frequently used because of their orthogonal properties. They lead to an elimination of the influence of the actual adjustment errors by matching the ray tracing program and the measured wavefront.[17] Fig. 18 shows a typical example where an aspheric surface was tested with a CGH with adjustment errors introduced. Fig. 18a shows the fringe patterns with two additional centring errors of 0,02 and 0,2 introduced and fig.18b represents the wavefront analysed with four different wavefronts with centring errors from 0,02 to 0,2 mm. The compensated wavefront with the centring errors is shown in fig. 18c indicating the shape error only.

6. Component and system analysis from interference patterns

Twyman-Green and Fizeau interference arrangements are frequently used for testing spherical and aspherical surfaces. By testing aspherical surfaces using computer generated holograms (CGH) for absolute measurement or by relative measurement using holographic techniques, the asphericity as well as the adjustment errors of the test surface need to be determined. Adjustment errors can be evaluated from the interferogram and compensated. By testing aspherical surfaces the coefficients of asphericity and adjustment errors of test surface and holograms can be determined from the interferograms. In a combined measuring procedure including ray tracing and fringe analysis a procedure for system analysis was developed including the following steps:

- automated fringe analysis
- development of the measured wavefront of the fringe pattern into polynoms
- considering polynom coefficients as goal for the optimization
- variation of the system parameter to obtain best agreement between measurements and calculations.

For the procedure at first the wavefront will be determined applying optical ray tracing techniques leading to a fringe system. Usually a departure of the measured wavefront of the actual system from the computed occurs because the system parameters are slightly different.

The aim is therefore not so much the optimization of the original system but to modify the system parameters in such a way that the measured wavefront can be obtained in order to find the parameter errors in the system.

Damped least square techniques are useful. The system parameters radius of curvature, refractive index centring errors among others are varied to obtain the measured wavefront. Zernike polynomials are very useful for system analysis. To compute the actual system starting with Zernike coefficients obtained from the fringe pattern we can write:

$$F_i = G_i \, (F_{zi} - F_{ai}) \qquad 16)$$

where F_i are the Zernike coefficients obtained from the fringe pattern.

G is a weighting factor.

and

F_{zi} and F_{ai} are targets and actual values respectively .

writing expression (16) and Taillor expansion

$$F_i = F_{oi} + \sum_{j=1}^{m} B_{ij} (x_j - x_{oj}) + ... \qquad 17)$$

By variation of the parameter to approach the target x_j the deviation from the departure of the different system parameters from the theoretical values can be found:

$B_{ij} = \frac{\delta F_i}{\delta x_j}$ is the sensitivity of the system by variation of parameters found from ray tracing.

$x_j - x_{oj}$ can be found by inverting of expression 17.

Usually the number of equations is larger than the number of parameters. Therefore, the merit function should lead to a minimum.

Some of our applications of component and system analysis were

- the analysis of adjustment errors when testing spherical and aspherical surfaces[17]
- determination of the asphericity coefficients and vertex curvature of contact lenses
- fine adjustments of air spacings in optical systems
- measuring of refractive index of the element of optical systems.

Adjustment errors occuring by the test procedure modify the fringe pattern. It should be noticed that by testing aspheric surfaces with CGH, seven degrees of freedom need to be considered. From the analysis of the fringe pattern the contribution of adjustment errors like centring errors can be calculated and subtracted from the wavefront. By subtracting adjustment errors, included typically in some coefficients of the polynomials the surface errors should not be affected. A typical result of adjustment error subtraction from an interferogram is shown in fig. 18.

Contactlenses will be selected and specified by the vertex curvature and the aspheric parameter, the excentricity of the back surface. The determination of such parameters from the fringe pattern is obtained with the procedure described in equation.[17] The measured wavefront will be described by Zernike polynomials up to the order 10. From the coefficients the vertex curvatures and aspheric coefficients are found by iteration leading to the best fit of the measured fringe pattern.

Furthermore from the fringe pattern not agreeing with the expected wavefront the errors such as centring errors or separations of lens components can be evaluated and compensated.

7. Engineering Application of Holographic Interferometry

Holography is a technique by which a wavefront of an object with an optically rough surface is recorded together with a reference wave. The reconstruction in the absence of the object leads to the same physical effect as the observation of the original object. Holographic interferometry enables the analysis of static and dynamic displacement of optically rough surfaces to be measured interferometrically. First reports of the method appeared 1965 and were soon followed by numerous papers describing new applications.[18,19]

The major applications of holographic interferometry are in measuring mechanical displacement, vibration, stress and deformation. Depending on the application, different techniques were developed. Double exposure, multiple and time average exposure techniques were introduced, as well as beam modulation and stroboscopic exposures.[17,18] In addition, fringe localizations together with fringe pattern analyses in three dimensional space have been investigated. By 1970, published material was available predicting the object motion from the fringe pattern. Methods were established to extract vectorial object displacement from the fringes, their parallax and their localization required in their applications. The search for simpler techniques fringe analysis in holographic interferometry initiated various studies.[22] The theories developed so far simplify the analysis and make it easier for the engineer to understand and apply it. Sometimes,

INTERFEROMETRY

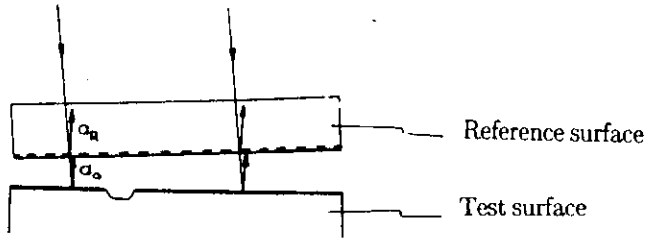

$$I = \left| a_R\, e^{\,i(wt - \phi_R)} + a_o\, e^{\,i(wt - \phi_o)} \right|^2$$

$$I = |a_R|^2 + |a_o|^2 + 2a_R a_o \cos(\phi_R - \phi_o)$$

$$\boxed{I = I_o \left\{ 1 + m \cos(\phi_R - \phi_o) \right\}}$$

$$I_o = |a_R|^2 + |a_o|^2$$

$$m = \frac{I_{max} - I_{min}}{I_{max} + I_{min}} = \frac{2 a_R a_o}{I_o}$$

= Modulation

$$\phi = \phi_R - \phi_o = \frac{2\pi}{\lambda}\; 2W(x_p', y_p')$$

2λ INTERFEROMETRY

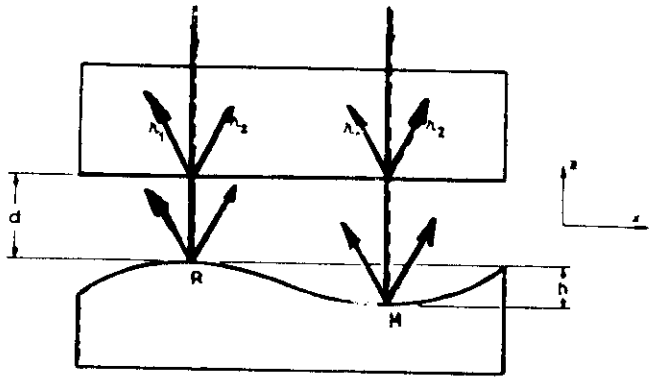

$$\Delta\phi_R = 2d\left(\frac{2\pi}{\lambda_1} - \frac{2\pi}{\lambda_2}\right)$$

in R:

$$\left.\begin{aligned} &2I_1(1 + \cos\phi_1) \\ &2I_2(1 + \cos\phi_2) \end{aligned}\right\} \Delta\phi_R = \phi_1 - \phi_2$$

in M:

$$\left.\begin{aligned} &2I_1(1 + \cos\phi_1 + \frac{4\pi}{\lambda_1} h) \\ &2I_2(1 + \cos\phi_2 + \frac{4\pi}{\lambda_2} h) \end{aligned}\right\} \Delta\phi_M = \phi_1 + \frac{4\pi}{\lambda_1}h - (\phi_2 + \frac{4\pi}{\lambda_2}h)$$

$$\Longrightarrow$$

$$\Delta\phi_M = \Delta\phi_R + \frac{4\pi h}{\lambda_1} - \frac{4\pi h}{\lambda_2}$$

$$\boxed{\Delta\phi_M = \Delta\phi_R + \frac{4\pi h}{\Lambda}}$$

$$\boxed{\Lambda = \frac{\lambda_1 . \lambda_2}{|\lambda_2 - \lambda_1|}}$$

$\lambda_1 = 514\text{nm}$, $\lambda_2 = 633\text{nm}$ $\Big\}$ $\Lambda = 2{,}73\mu\text{m}$

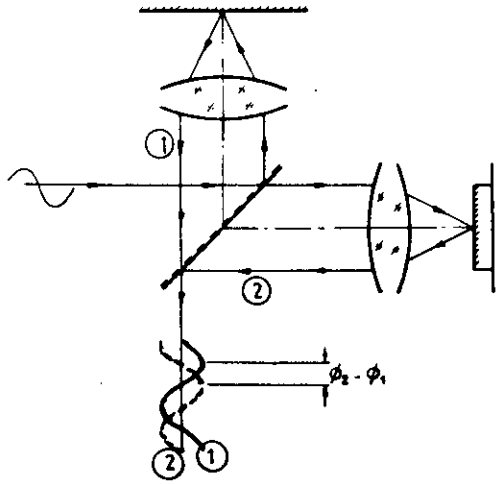

$$a\cos(\omega t - \phi) = \mathrm{Re}(a.e^{i(\omega t - \phi)})$$

$$\langle I \rangle_T = \langle |a_1.e^{i(\omega t - \phi_1)} + a_2.e^{i(\omega t - \phi_2)}|^2 \rangle_T$$

$$I = \{|a_1|^2 + |a_2|^2\} + 2a_1a_2\cos(\phi_2 - \phi_1)\}$$

$$\phi_1 = \frac{2\pi}{\lambda} l_1 \qquad \phi_2 = \frac{2\pi}{\lambda} l_2$$

$$\Delta\phi = \frac{2\pi}{\lambda}(l_2 - l_1)$$

$$\boxed{I = I_0\{1 + m\cos\Delta\phi\}}$$

$$I_0 = |a_1|^2 + |a_2|^2$$

$$m = \frac{2a_1a_2}{|a_1|^2 + |a_2|^2}$$

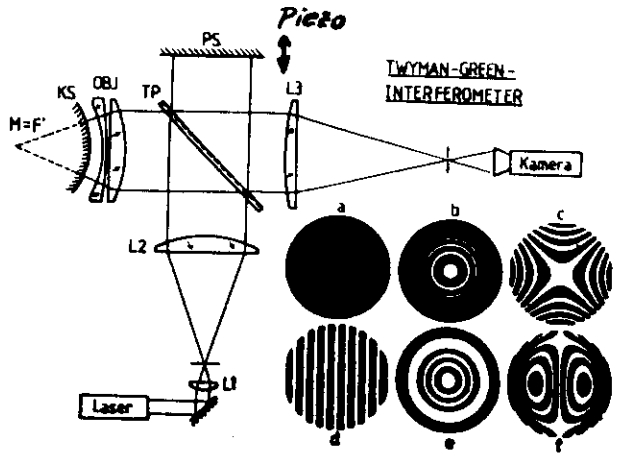

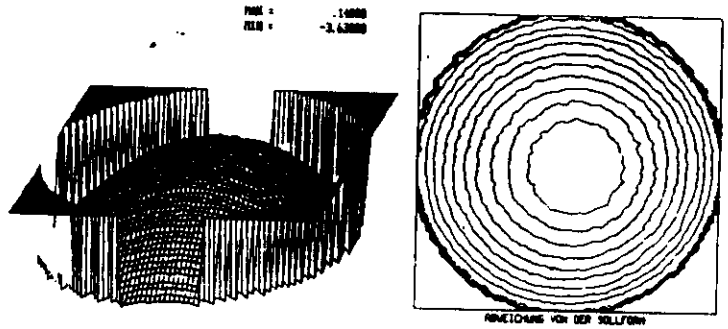

FRINGE ANALYSIS

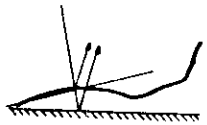

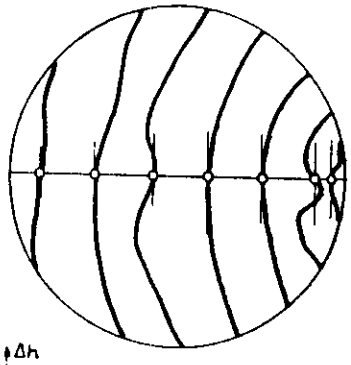

$$\Delta\phi = \frac{4\pi}{\lambda}\Delta h$$

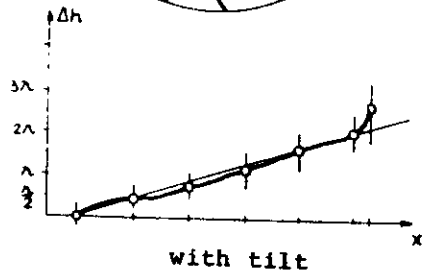

with tilt

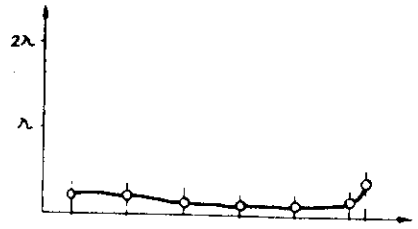

without tilt

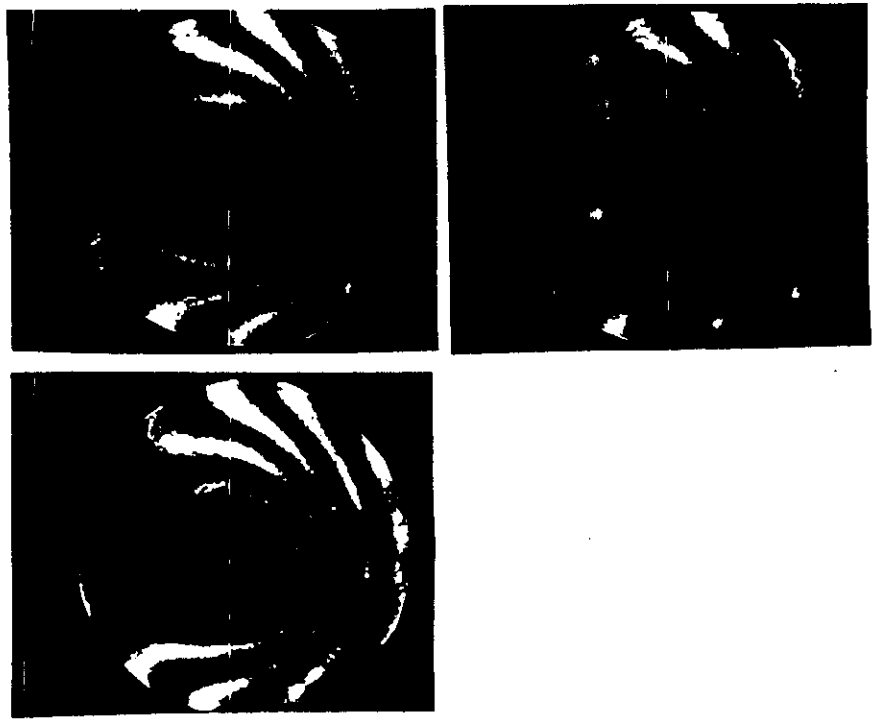

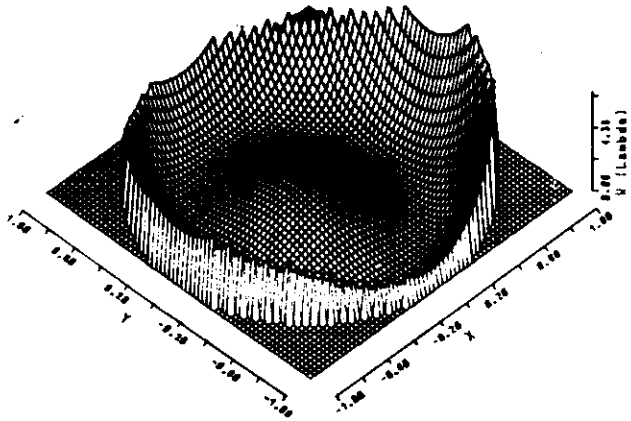

Interferogram with tilt

Fourier-Spectrum

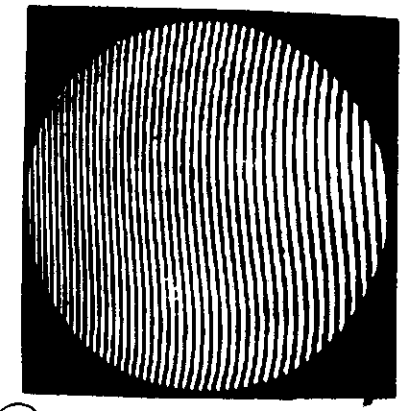

a

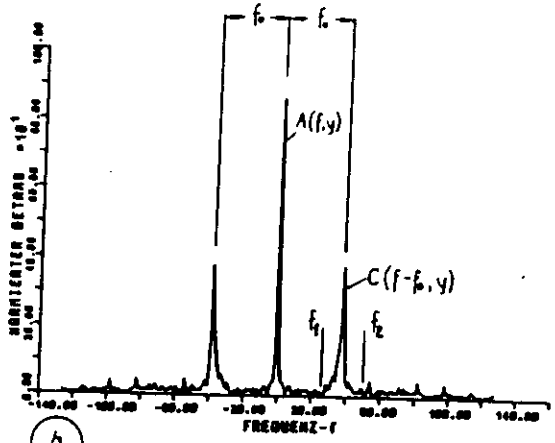

b

Fig. 1

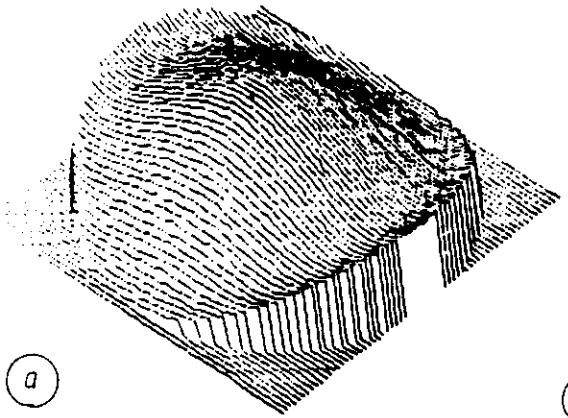

a

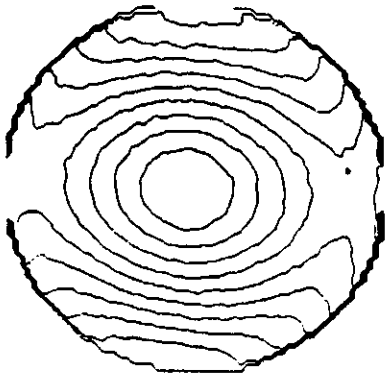

b

PV : 5.449
RMS: 1.244
TLT 3.212/3.537°

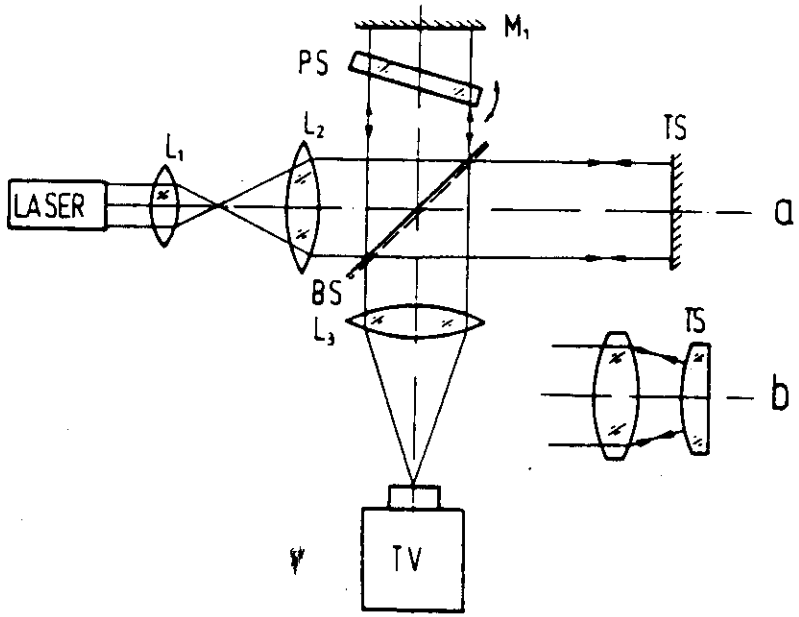

Fig. 3

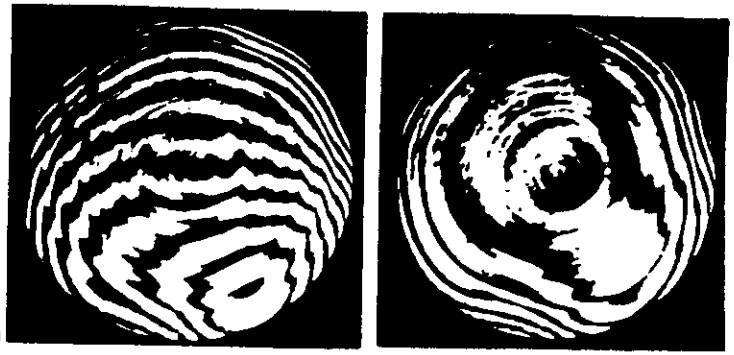

a

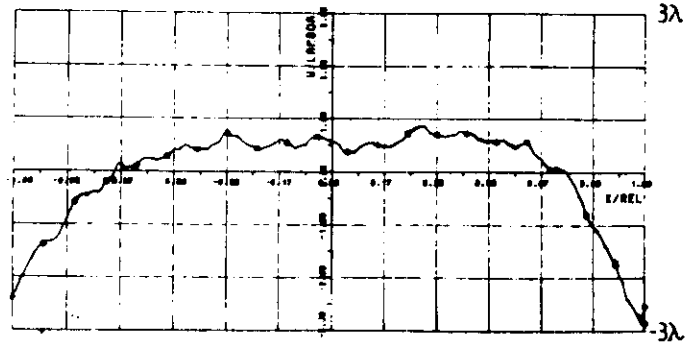

b

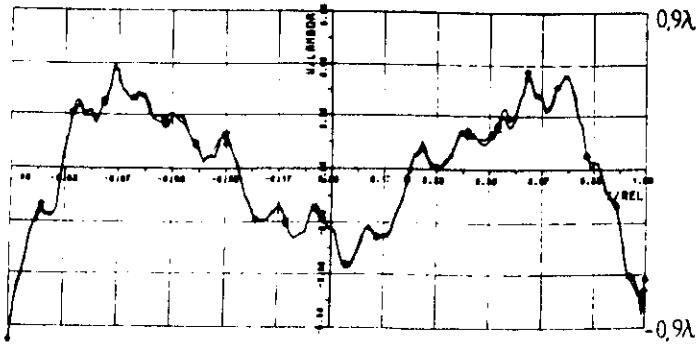

c

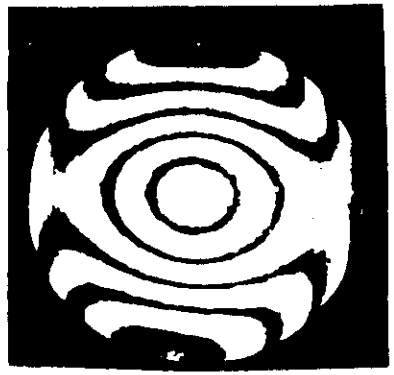

a

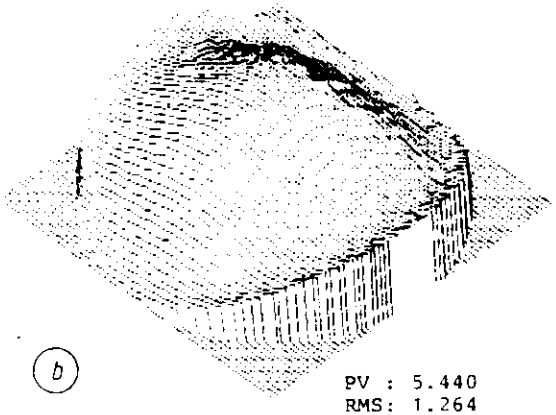

b

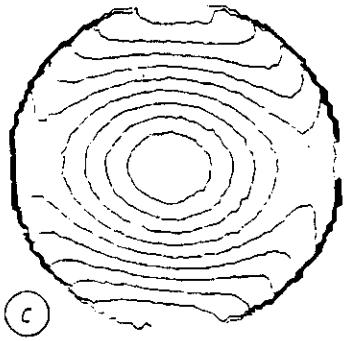

c

PV : 5.440
RMS: 1.264
TLT 20.042/80.293°

Fig. 5

FRINGE ANALYSIS

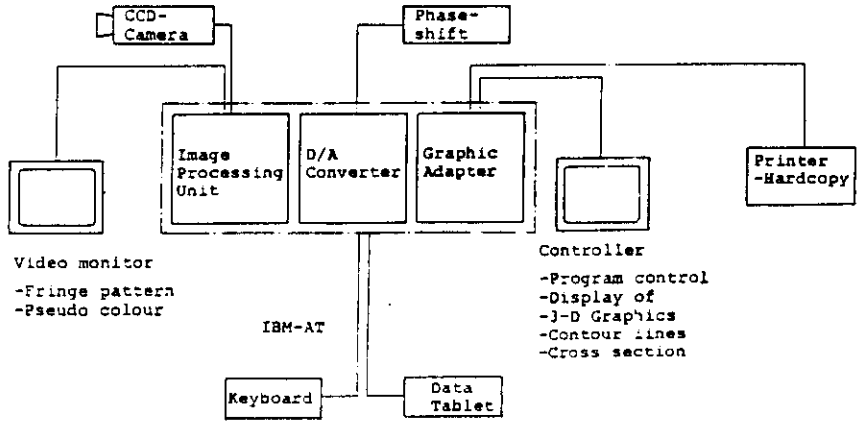

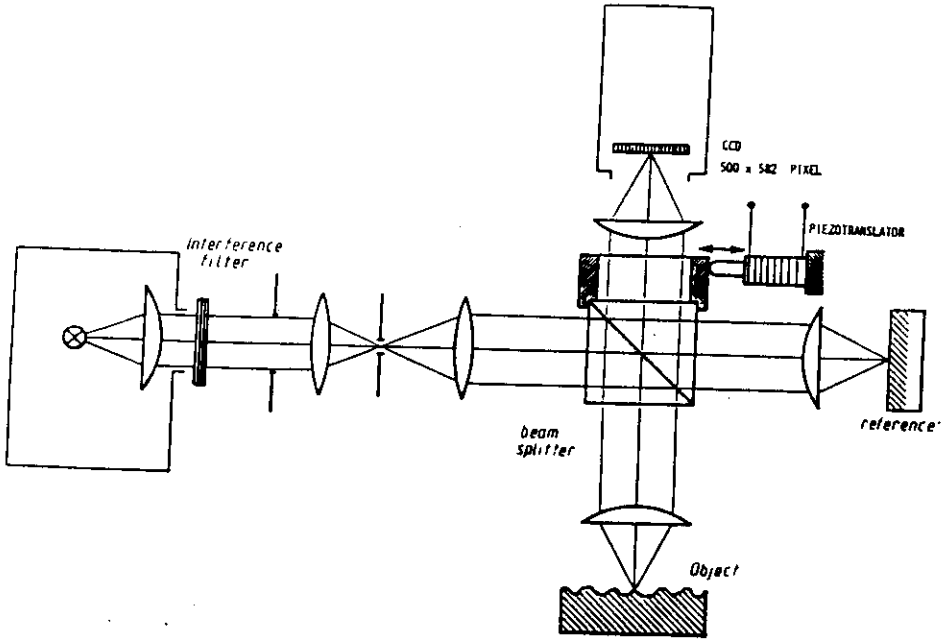

Fig. 7

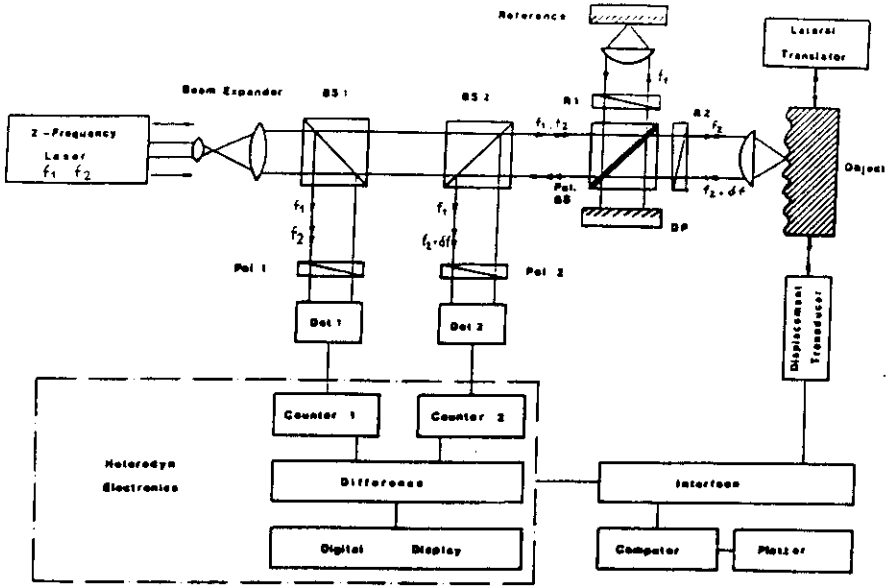

Fig. 9

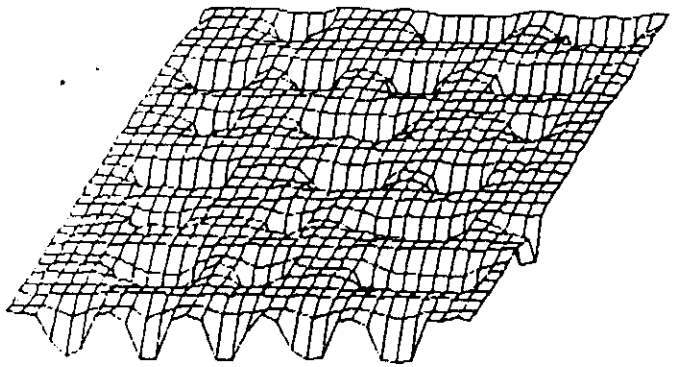

Fig. 8

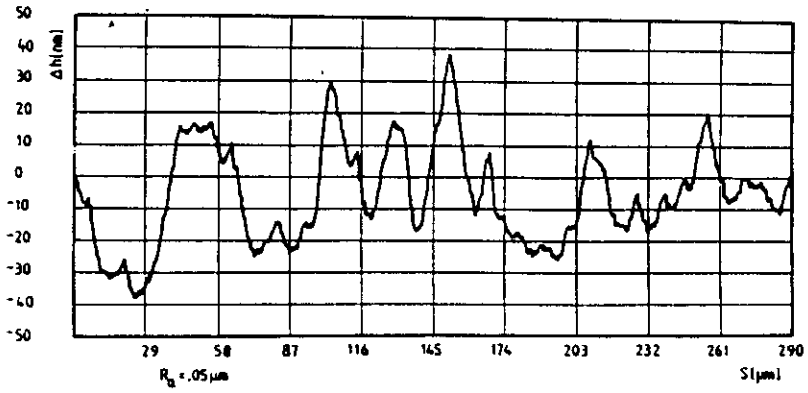

Fig. 10

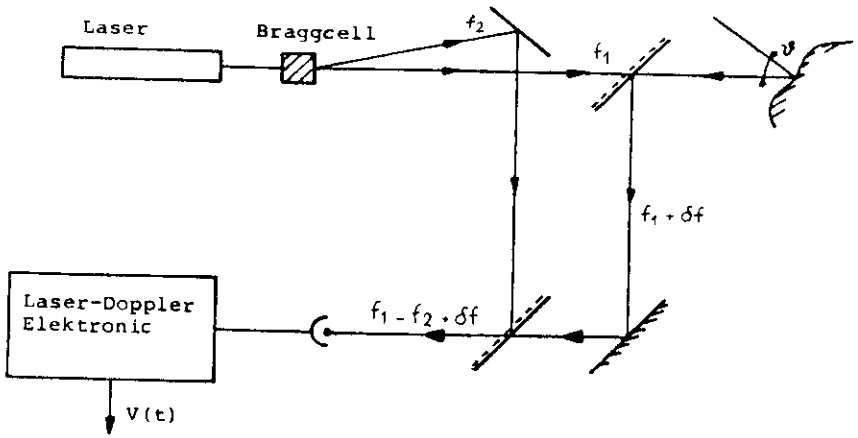

Fig. 11

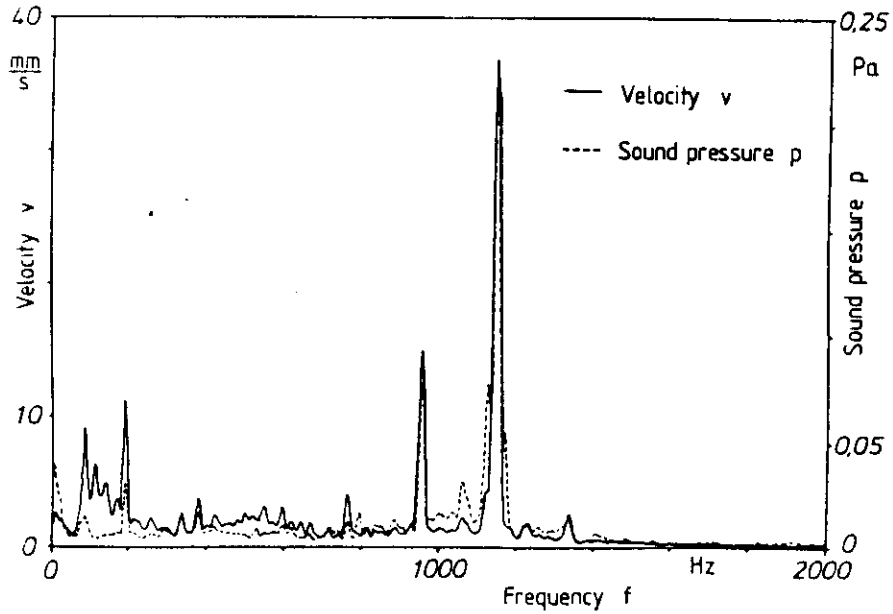

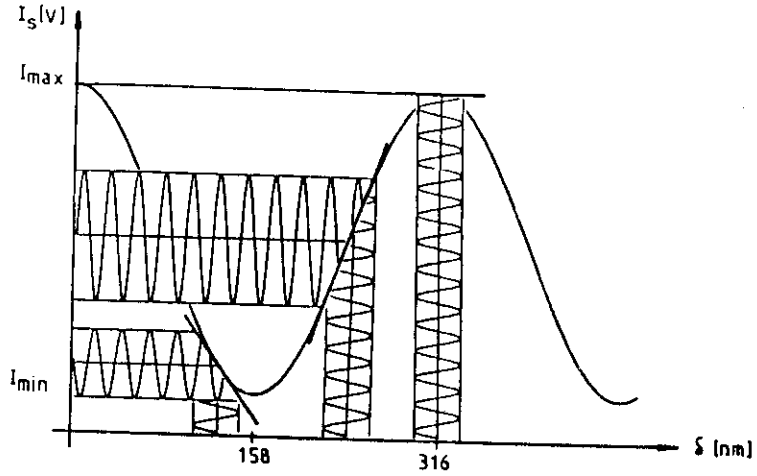

Fig. 13

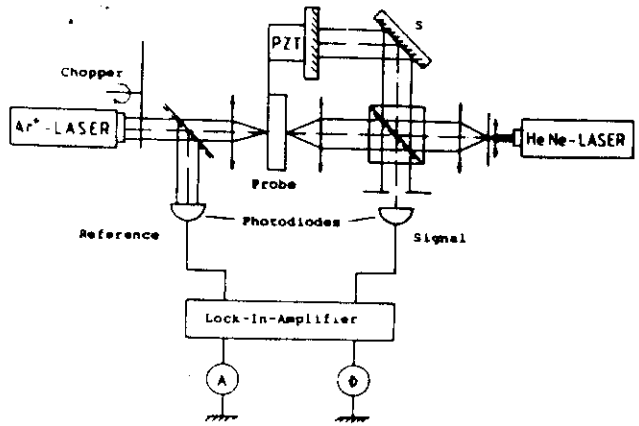

Fig. 14

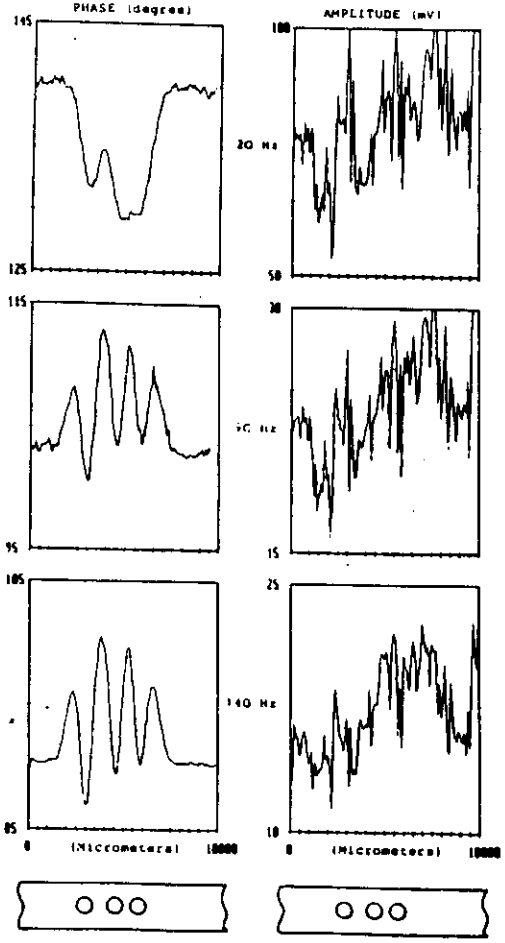
PHASE (degree)
AMPLITUDE (mV)
145
125
100
50
20 Hz
115
95
30
15
60 Hz
105
85
25
10
140 Hz
0
(Micrometers)
10000
0
(Micrometers)
10000

Fig. 15

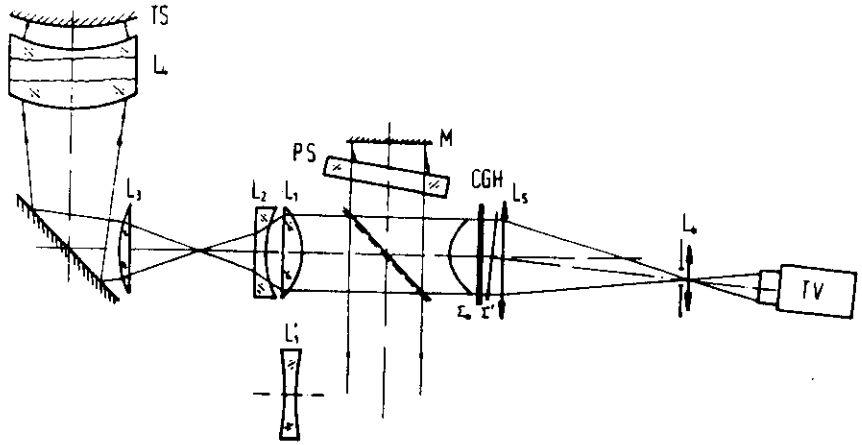
TS
L4
PS
M
L3
L2
L1
CGH
L5
L4
TV
L'1

Fig. 16

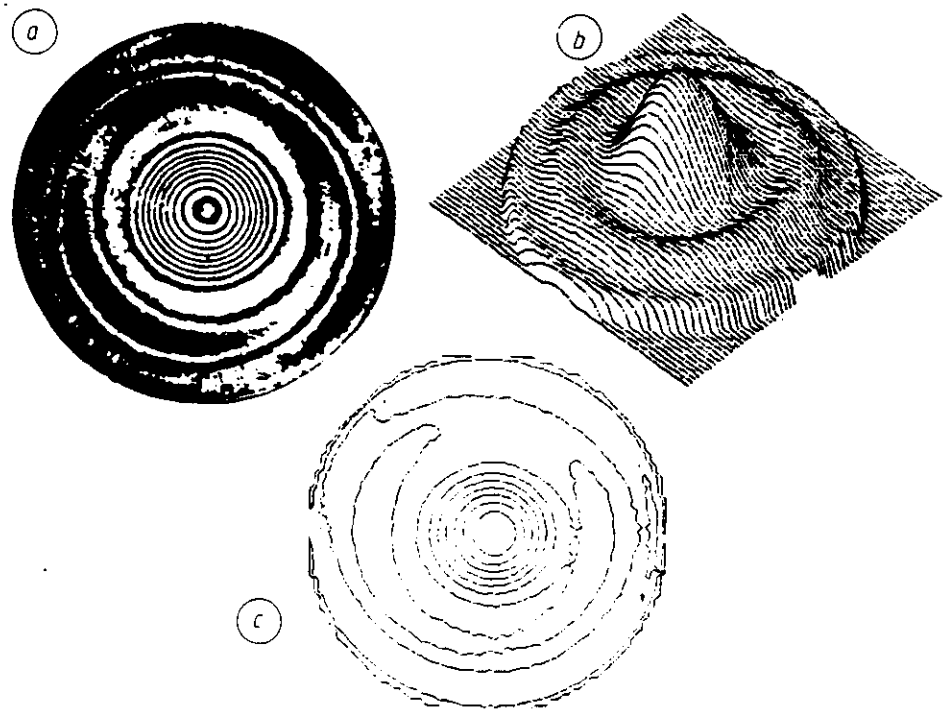
a
b
c

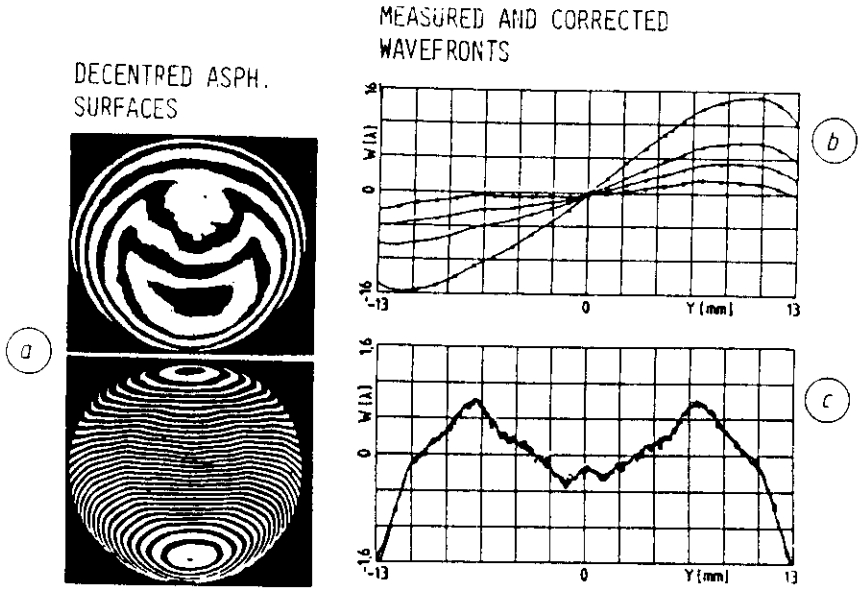

Fig. 18

References

1. R. DÄNDLIKER, in 'Progress in Optics', Vol. XVII, edited by E. Wolf (North-Holland, Amsterdam, 1980) p. 1.
2. M. TAKEDA, H. INA and S. KOBAYASHI, *J. Opt. Soc. Am.* **72** (1982) 156.
3. TH. KREIS, *J. Opt. Soc. Am.* **A3** (1986) 847.
4. J. H. BRUNNING, in 'Optical Shop Testing', edited by D. Malacara (Wiley, New York, 1978) 409.
5. B. DÖRBAND, *Optik* **60** (1982) 161.
6. J. SCHWIDER, R. BUROW, K. E. ELSNER, J. GRZONNA, R. SPOLACZYK and K. MERKEL, *Appl. Opt.* **22** (1983) 3421.
7. J. C. WYANT, C. L. KOLIOPOULOS and B. BUSHBAN, *ASCE Trans.* **27** (1984) 101.
8. K. CREATH, *Proc. SPIE* **680** (1986).
9. F. M. KÜCHEL, TH. SCHMIEDER and H. J. TIZIANI, *Optik* **65**, (1983) 123.
10. H. J. TIZIANI, in 'Rechnerunterstützte Laser-Meßtechnik', Technisches Messen, Vol. 54 (1987) 221.
11. B. DÖRBAND and H. J. TIZIANI, *Appl. Opt.* **24** (1985) 2604.
12. C. C. HUANG, *Opt. Engng* **23** (1984) 365.
13. S. E. GREIVENKAMP, *ibid.* **23** (1984) 350.
14. K. LEONHARDT, K.-H. RIPPERT and H. J. TIZIANI, in 'Optische Profilometrie und Rauheitsmessung', Technisches Messen, Vol. 54 (1987) 243.
15. U. ESSERS, R. EBERSPÄCHER, W. LIEDL, R. LITSCHEL, B. PFISTER, H. J. TIZIANI and A. ZELLER, 'Entwicklungslinien in Kraftfahrzeugtechnik und Straßenverkehr' (Verlag TÜV Rheinland, Köln, 1981).
16. G. BUSSE, *IEEE Trans. Sonics Ultrasonics* **SU-32** (1985) 355.
17. Z. SODNIK and H. J. TIZIANI, *Opt. Commun.* **58** (1986) 295.
18. W. SCHUMANN and M. DUBOIS, 'Holographic Interferometry', Springer Series in Optical Science, Vol. 16 (Springer-Verlag, Berlin, 1975).
19. R. JONES and C. WYKES, 'Holographic and Speckle Interferometry' (Cambridge University Press, 1983).
20. B. BREUCKMANN and W. THIEME, *Appl. Opt.* **24** (1985) 2145.